Eur. Phys. J. B **31**, 3–9 (2003)
DOI: 10.1140/epjb/e2003-00001-3

THE EUROPEAN PHYSICAL JOURNAL B

Studies on CdS nanoparticles dispersed in silica matrix prepared by sol-gel technique

B. Bhattacharjee, S.K. Bera, D. Ganguli, S. Chaudhuri, and A.K. Pal[a]

Department of Materials Science, Indian Association for the Cultivation of Science, Calcutta 700 032, India

Received 24 May 2002
Published online 27 January 2003 –

Abstract. SiO_2/CdS-nanoparticle composite films (SiO_2:CdS=85:15, 80:20, 75:25 and 70:30) were prepared by the sol-gel route. The films were characterized by studying microstructural (XRD and TEM) and optical (transmittance and photoluminescence) properties. Band gaps of these films annealed at different temperatures (373–473 K) for different times (10–120 min) indicated that the signature of nanocrystallinity is retained throughout the range of our experimental conditions. A thermal diffusion process controlled growth in the crystallite size with increasing annealing time and temperature. The average radii of the nanoparticles varied as the cube root of the annealing time but showed exponential dependence on the inverse of annealing temperature. Photoluminescence (PL) studies of the composite films indicated excitonic transitions. Theoretical analysis of the line shapes of the PL peaks recorded at 300 K and 80 K could be accounted for by the combined effects of size distribution and phonon broadening. It was observed that the deformation potential (E_d) effectively controlled the line shapes of the PL measurements.

PACS. 78.20.-e Optical properties of bulk materials and thin films – 81.05.Dz II-VI semiconductors

1 Introduction

II-VI binary semiconductors like ZnTe, ZnS, CdTe, CdSe and CdS received much attention due to their various potential applications [1–6]. Among them, CdS and CdSe doped glasses were found to be useful for optical communication and optical signal processing [5]. Different physical and chemical synthesis routes were adopted by different workers for the preparation of nanostructures of compound semiconductors. High pressure magnetron sputtering seemed to be a very useful technique for preparing tailored nanocrystalline thin films of CdSe embedded in a SiO_2 matrix [7,8]. However, sol-gel processing emerged as an attractive alternative for the fabrication of such composite films utilizing combinations of II-VI semiconductors and dielectrics like SiO_2 [6,9], TiO_2 [10], and ZrO_2 [11]. Banerjee *et al.* [12] synthesized CdS nanoparticles *via* precipitation from an aqueous solution containing $CdCl_2$, thiourea and ammonia and they indicated that optical properties of nanocrystalline CdS were governed by not only quantum confinement effect but also its structural phase transition from wurtzite to zinc blende structure. Nogami *et al.* [13] reported their studies on CdS doped silica glass prepared by sol-gel process and identified hexagonal wurtzite CdS crystals of 2 to 6 nm diameter by XRD and TEM studies. CdS particles in silica glasses were prepared by Cordoncillo *et al.* [14] by sol-gel technique. Samples fired at 623 and 773 K showed absorption edges at 460 nm and 430 nm respectively. Size effects in the excited electronic states of small colloidal CdS crystallites were also studied by Rossetti *et al.* [15] as a function of crystallite size.

In this communication, we report the preparation of composite films of SiO_2:CdS in which nanoparticles of CdS with relatively high molar ratio (Refs. [6,9] for comparison) was embedded in SiO_2 matrix by the sol-gel technique. The films were characterized by microstructural (XRD and TEM) and optical (transmittance and photoluminescence) studies.

2 Experimental details

In a typical preparative protocol, silica sol was first prepared by dissolution of tetraethyl orthosilicate, $Si(OC_2H_5)_4$ (TEOS, for synthesis, Merck.Schuchardt) in 2-propanol, $(CH_3)_2CHOH$ (GR, Merck India) dried over activated molecular sieve Zeolite 4A and addition of distilled water. Hydrochloric acid (0.1N) (Titrisol, Merck India) was added as catalyst. A solution of $Cd(NO_3)_2{\cdot}4H_2O$ (Purified, Merck India) and thiourea, NH_2CSNH_2 (Pure, Merck India) as sources for Cd and S respectively was also prepared separately in 2-propanol

[a] e-mail: msakp@mahendra.iacs.res.in

and distilled water. This solution was slowly added to the silica sol under vigorous stirring. The final sol thus prepared was stirred for 1–2 h. The equivalent molar ratios of SiO_2:CdS in the prepared sols varied in the range of 85:15, 80:20, 75:25 and 70:30 with sol composition in the molar ratio H_2O: TEOS: $(CH_3)_2CHOH$: $Cd(NO_3)\cdot 4H_2O$: NH_2CSNH_2=5:1:17.2:0.15-0.45:0.15–0.45.

The sols were used for spin coating (∼3000 r.p.m.) on properly cleaned soda lime glass substrates (25 mm × 25 mm). The coated substrates were transferred immediately after coating into a tubular oven previously set at the required temperature (373–473 K). The annealing time was varied in the range of 10–120 min. For each investigation, a series of gel films, all prepared under identical conditions and having very similar characteristics (*e.g.* optical transmittance), were first prepared (as deposited films), which were then annealed under different conditions as outlined above.

The films were characterized by recording optical transmittance *versus* wavelength traces by a spectrophotometer (Hitachi U 3410). Microstructural studies were carried out by transmission electron microscopy (Philips CM-200) and X-ray diffractometry (Philips PW 3719). Photoluminescence (PL) measurements were carried out in the temperature range of 80–300 K by using a 300 W xenon arc lamp as the emission source. A Hamamatsu photomultiplier was used as the detector along with a 1/4 m monochromator. The spectra were recorded with excitation at 400 nm radiation.

3 Results and discussion

3.1 Optical transmittance and microstructural studies

Films of nanocrystalline CdS embedded in SiO_2 matrix with different CdS content were prepared by varying the relative molar ratio of SiO_2 and CdS in the sol. All the as-deposited films were colourless. The films turned pale yellow when annealed above 350 K. and the colouration was more pronounced for films with higher CdS content. The as-deposited films were subjected to annealing at different temperatures and time to study the evolution of CdS nanoparticles in SiO_2 matrix and the physical properties of the resultant films. It may be noted here that increase in annealing temperature had more pronounced effect in the evolution of CdS nanocrystallites than duration of annealing.

A number of films were deposited at room temperature with SiO_2:CdS=70:30 under identical condition. The as-deposited films were annealed at different temperatures ranging between 373–473 K keeping the annealing time ∼60 min. Figure 1 shows transmission (T_r) *vs.* wavelength (λ) traces for the representative films prepared as above. It may be observed that the transmittance of the as-deposited film (curve a) did not show any fall indicating the absence of formation of CdS nanocrystals in this film. As the film was annealed at higher temperature (∼373 K), one can observe distinct fall in transmittance spectra (curve b) near the band gap energy of CdS.

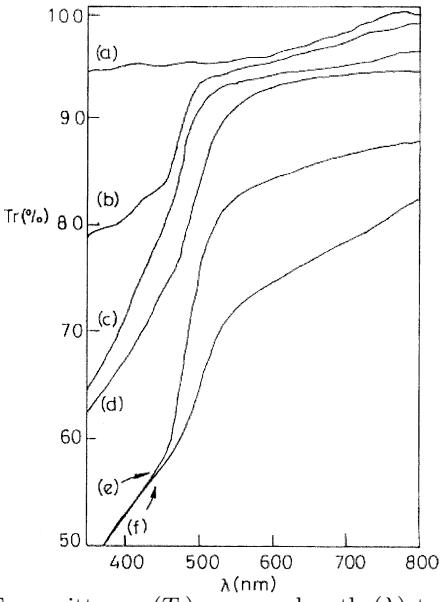

Fig. 1. Transmittance (T_r) *vs.* wavelength (λ) traces for six representative films with SiO_2:CdS=70:30 annealed for 60 minutes at different annealing temperatures: (a) as-deposited; (b) 373 K; (c) 393 K; (d) 433 K; (e) 453 K and (f) 473 K.

The fall became sharper (curves c, d, e and f) when the films were annealed at increasing annealing temperatures. It may be observed that the films became more absorbent and the fall in the transmittance at the band edge became sharper with increasing annealing temperature. A distinct reduction in blue shift of the band gap due to quantum size effects could also be observed. This behaviour could be attributed to the coalescence of the adjacent nanocrystallites with the increase in annealing temperature. The effect of coalescence would culminate in an increase in crystallite size at the expense of number density of the nanocrystallites constituting the film. For films with increasing CdS content, one would expect an increase in the number of adjacent crystallites which would favour coalescence culminating in increased size of the nanocrystallites. Thus, at higher annealing temperature one would expect enhanced coalescence in the films having higher CdS content which is in conformity with the observation on the films with higher CdS content (discussed in detail later and shown in Fig. 6). Also, with the increase in annealing temperature possibility of compressive stress due to large difference in the coefficient of thermal expansion of substrate (sodalime glass)/SiO_2 and nanocrystallites (CdS) would appear in the film which would also favour the reduction in blue shift for films synthesized at higher annealing temperature.

Figure 2 shows the glancing angle XRD for the above representative films. The as-deposited film showed characteristic peaks for thiourea (not shown here) which had crystallized out of the sol during drying of the film at room temperature. No characteristic peaks for CdS were obtained for this film, which is consistent with the optical result. Peaks for nanocrystalline CdS for reflections from (002) planes started appearing (Figs. 2a–c) as the annealing temperature is increased. Distinct peaks for reflections

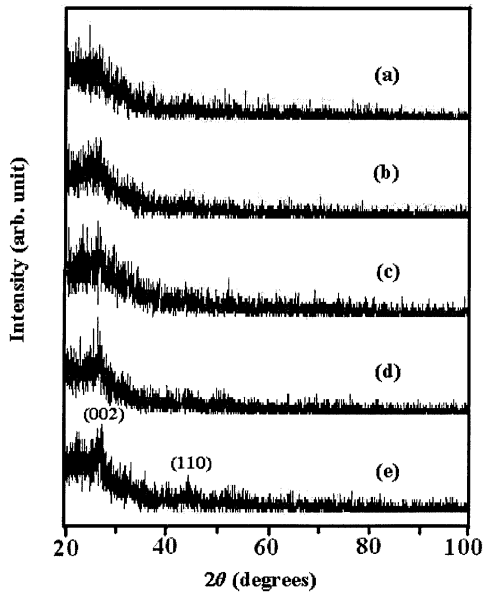

Fig. 2. Small angle XRD traces for representative films with SiO_2:CdS=70:30 annealed at: (a) 350 K; (b) 373 K; (c) 400 K; (d) 450 K and (e) 473 K.

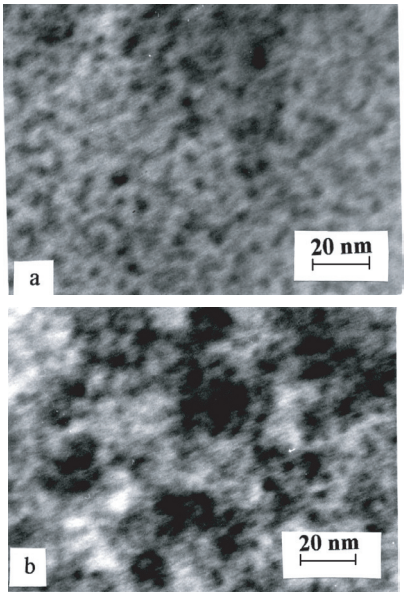

Fig. 3. TEM micrographs of two representative films with SiO_2:CdS=85:15 annealed at: (a) 373 K and (b) 473 K.

from hexagonal CdS (002) at $2\theta \sim 26.6°$ appeared for films annealed at 373 K for 60 min (Fig. 2, curve b). As the annealing temperature is increased, the peak became sharper (indicated by the decrease in FWHM) and another peak for (110) located at $2\theta = 44.17°$ could be observed (Fig. 2, curve e) for the film annealed at higher temperature (∼473 K). It may also be noted that with increasing CdS content in the films, the peaks became sharper and intense with no other observable distinction in the XRD spectrum.

Signature of coalescence could be distinctly observed from the TEM micrographs of two representative films shown in Figure 3. Figures 3a and b show the micrographs of a representative film with SiO_2:CdS=85:15 annealed at 373 K and 473 K for 60 min respectively. One can observe that appearance of distinct CdS nanocrystallites is visible (Fig. 3a) for the film annealed for 60 min and coalescence could be observed (Fig. 3b) if the annealing temperature is increased to 473 K. A similar effect of coalescence was observed for films with different CdS content annealed at higher annealing temperature.

The absorption coefficients (α) were calculated from the transmittance data and optical band gaps (E_g) were determined by extrapolating the straight line portion [16,17] of the $(\alpha h\nu)^2$ *vs.* $h\nu$ plot to $\alpha = 0$. The optical absorption coefficient (α) may be expressed as [16,17]:

$$\alpha = (A/h\nu)\{h\nu - E_g\}^m \qquad (1)$$

where, $h\nu$ is the incident photon energy, A is a constant depending on the nature of transition which is also reflected in the value of m. Now, equation (1) may be rewritten as

$$\ln(\alpha h\nu) = \ln A + m\ln(h\nu - E_g) \qquad (2)$$

and

$$[\mathrm{d}(\ln(\alpha h\nu))/\mathrm{d}(h\nu)] = m/(h\nu - E_g)\cdot \qquad (3)$$

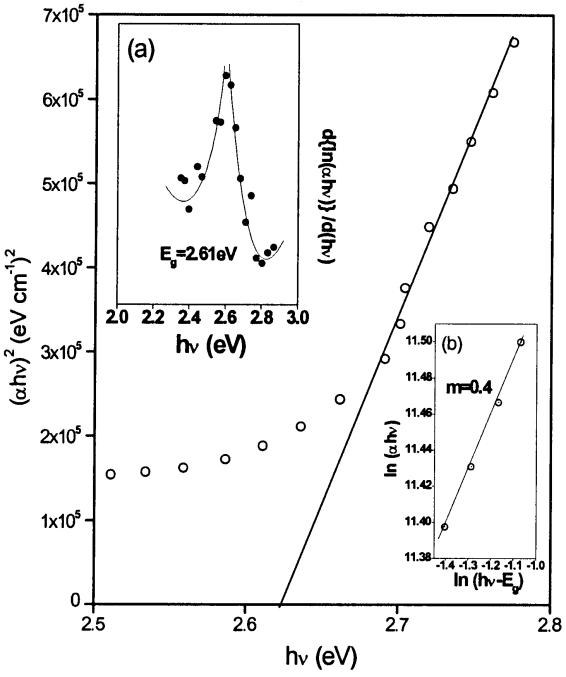

Fig. 4. Plot of $(\alpha h\nu)^2$ *vs.* $h\nu$ for a representative film; Inset (a) shows the plot of $\mathrm{d}\{\ln(\alpha h\nu)\}/\mathrm{d}(h\nu)$ *vs.* $h\nu$; Inset (b) shows plot of $\ln(\alpha h\nu)$ *vs.* $\ln(h\nu - E_g)$.

Equation (3) suggests that a plot of $[\mathrm{d}\{\ln(\alpha h\nu)\}/\mathrm{d}(h\nu)]$ *vs.* $h\nu$ will indicate a divergence at $h\nu = E_g$ from which the value of E_g may be obtained. Inset (a) of Figure 4 shows the plot of $[\mathrm{d}\{\ln(\alpha h\nu)\}/\mathrm{d}(h\nu)]$ *versus* $h\nu$ for a representative film. This showed a discontinuity from which we can identify a transition at ∼2.61 eV. Using equation (2), the nature of transition (*i.e.*. the value of m) could be obtained unambiguously from the slope of the plot of $\ln(\alpha h\nu)$ *vs.* $\ln(h\nu - E_g)$ as shown in the inset 'b' of Figure 4. The

Table 1. Band gap and particle radii for SiO_2:CdS composite films with different compositions annealed at 473 K for 60 minutes.

SiO_2:CdS (molar ratio)	E_g (eV) (From optical measurements)	Particle radius (nm) (From band gap shift)	Particle radius (nm) (From TEM)	Particle radius (nm) (From PL fit)
85:15	2.49	7.9	7.8	7.9
80:20	2.46	8.0	8.1	8.1
75:25	2.45	8.4	8.5	8.5
70:30	2.43	8.8	8.8	8.9

values of m obtained as above were slightly less than 0.5 (varied between 0.40 and 0.48) which are the signature of allowed direct transitions in the films. The exact values of E_g of the films obtained by extrapolating the straight line portions of the plots of $(\alpha h\nu)^2$ *vs.* $h\nu$ to $\alpha = 0$ (Fig. 4) are shown in Table 1. These E_g values were greater than the bulk value of CdS ($E_g = 2.4$ eV). This blue shift in the band gap could be attributed to quantum confinement due to nanocrystalline nature of CdS in the films.

The radii r of the CdS nanocrystallites obtained from TEM studies for films annealed at different temperatures (373–473 K) varied between 3.7–9 nm. Thus, the values of r were always greater than or nearly equal to the Bohr radius ($a_B \sim 3$ nm) [18]. Then, for weak confinement limit (*i.e.*, $r \gg a_B$), we have [19,20]:

$$E_g = E_g^o + \frac{\hbar^2\pi^2}{2Mr^2} - E_{RY}^* \cdot \qquad (4)$$

In equation (4), r is the radius of the nanocrystallites, $E_{RY}^*(= e^2/4\pi\varepsilon\varepsilon_o a_B)$ is the effective Rydberg energy for the bulk exciton where $a_B = 4\pi\varepsilon\varepsilon_o\hbar^2/\mu e^2$, $\mu = [m_e m_h/(m_e + m_h)]$ being the electron-hole reduced mass. E_g^o and ε are the band gap and low frequency dielectric constant respectively of the bulk material. $M = m_e + m_h$, where m_e and m_h are the electron and hole effective masses respectively. Utilizing the average values of particle size $\bar{r}$, obtained from TEM measurements, the E_g values of different films were estimated from the above equation which were found to agree well with those obtained directly from the absorption spectra. Now, equation (1) indicates that the plot of $\Delta E_g\,(= E_g - E_g^o)$ *vs.* $1/r^2$ would be linear (Fig. 5) and the values of $M\,(= m_e + m_h)$ and E_{RY}^* may be obtained form the slope and intercept of the above plot which in turn would give the values of μ. The values of m_e and m_h obtained from M and μ were 0.26 m_0 and 0.44 m_0 (m_0 is the free electron mass) respectively which compare favourably with those obtained [21] for CdS. It may be noted from Figure 5 that excepting the data points for $r \sim a_B$ where neither the condition for weak or strong confinement holds good, the fit of the experimental data with equation (4) was in general quite satisfactory.

Ekimov *et al.* [22] showed that if the particles in a supersaturated solid grow by the diffusion process, growth of the average radius $\bar{r}$ of the particles depended on both annealing time t and temperature T as:

$$\bar{r} = [(4\beta Dt)/9]^{1/3} \qquad (5)$$

$$D = D_0 \exp(-\Delta E/KT) \qquad (6)$$

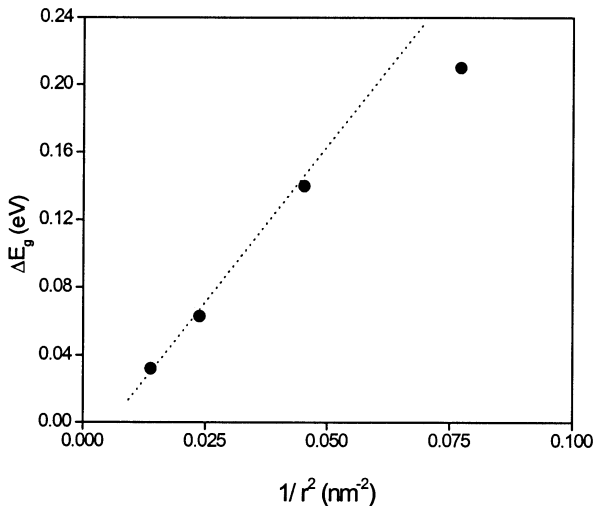

Fig. 5. Plot of ΔE_g *versus* $1/r^2$.

where D and ΔE stand for diffusion coefficient and activation energy respectively. β is a coefficient which is determined by the interfacial tension. Combining equations (5) and (6), we can write:

$$\bar{r} = [(4\beta D_0 t)/9]^{1/3} t^{1/3} \exp(-\Delta E/3KT) \cdot \qquad (7)$$

Equation (7) suggests that the radii ($\bar{r}$) of the particles increase in proportion to the cube root of annealing time (t), but would show an exponential dependence with the inverse of annealing temperature ($1/T$). Figure 6 shows the plots of $\bar{r}$ *vs.* $t^{1/3}$ for two different CdS contents (curves a and b). A linear variation of $\bar{r}$ *vs.* $t^{1/3}$ could be observed as suggested by equation (7). $\bar{r}$ *vs.* $1/T$ plots (curves c and d) for the same films show exponential dependence which is also consistent with equation (7). This observation is similar to that of Arai *et al.* [23]. Interestingly, films with higher CdS volume fraction (SiO_2:CdS$\sim$70:30) tend to lose nanocrystalline signature through enhanced coalescence at a faster rate (Figs. 6a and c) than those for films with lower CdS content both with increased annealing temperature (Figs. 6c and d) and time (Figs. 6a and b). Films with lower CdS content will have lower number density of the nanocrystallites which would facilitate in complete capping of them by SiO_2 and the distance among the nanocrystallites may not be favourable for possible coalescence with the adjacent ones through the SiO_2 barrier. As the number density of CdS nanocrystallites

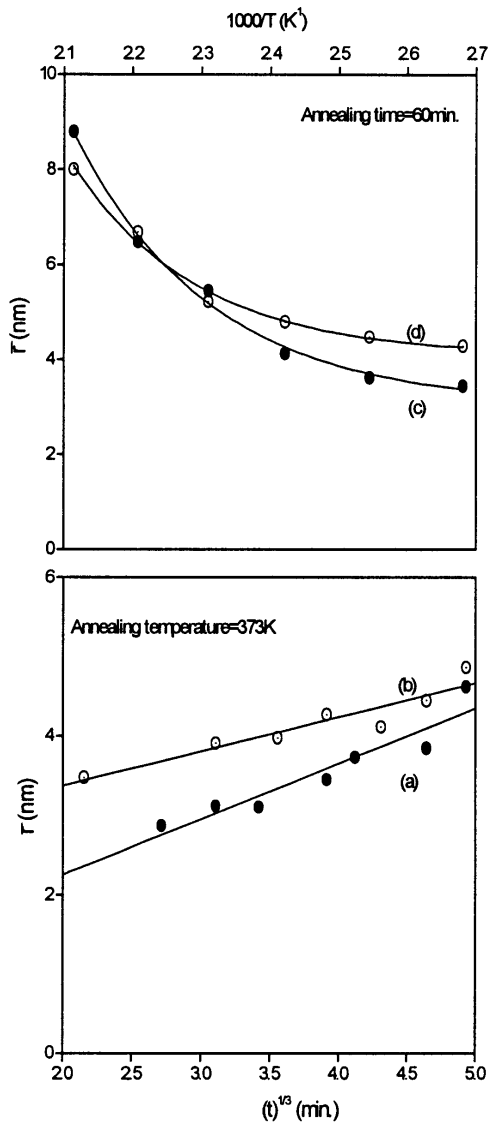

Fig. 6. Variation of average radius ($\bar{r}$) of nanocrystallites with annealing time (a and b) and inverse of annealing temperature (c and d) for films with different CdS contents: (○ - SiO_2:CdS=85:15 and ● - SiO_2:CdS=70:30).

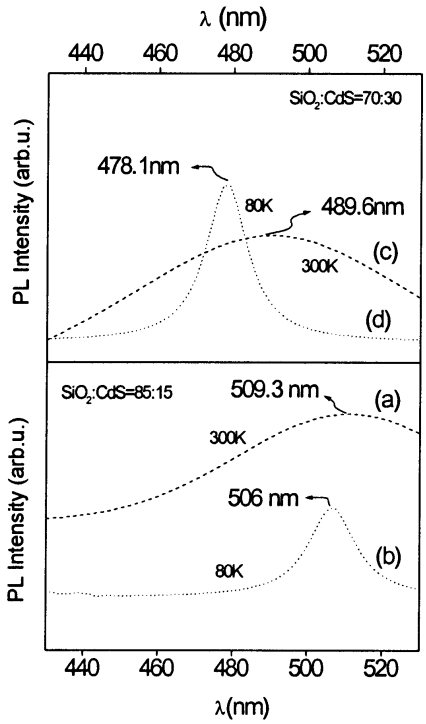

Fig. 7. Photoluminescence spectra for two representative SiO_2:CdS films with SiO_2:CdS=85:15 (a and b) and SiO_2:CdS=70:30 (c and d) annealed at 373 K for 60 min and recorded at 80 K (.....) and 300 K (-----).

increased with increase in CdS content in the film, the distance of the two adjacent nanocrystallites would also decrease. This would facilitate coalescence with increasing in annealing temperature or duration of annealing for forming larger crystallites. This is evident from the variation of nanocrystallite size $\bar{r}$ with annealing time t and annealing temperature T as shown in Figure 6.

3.2 Photoluminescence studies

Figure 7 shows typical PL spectra for two representative films with two different CdS contents (SiO_2:CdS=85:15 and 70:30) recorded at 80 K and 300 K. The PL spectra (a and c) at room temperature (300 K) may be seen to be dominated by broad peaks located near ∼510 and 490 nm for films with lower and higher CdS content respectively. Broadening of the room temperature spectra may be ascribed due to phonon broadening. The peak position shifted to lower wavelength when the spectra were recorded at lower temperature (80 K). This shift may be observed to be higher for the film with higher CdS content (curves c and d: peak shift ∼11 nm) than that for lower CdS content (curves a and b: peak shift ∼3 nm). The effect of surface states is quite visible from the broader PL peak for film with higher CdS content which would give rise to larger number of surface states from increased number of nanocrystallites residing at the surface.

The line shape of the PL spectrum is essentially given by the inhomogeneous broadening which is due to the size distribution of the crystallites. The theoretical line shape $I(\hbar\omega)$ of the PL spectrum between the lowest energy state of the electron and hole ($1s_e \rightarrow 1s_h$) in a quantum dot with radius r may be expressed as [24]

$$I(\hbar\omega) \propto \int g(r)|f(r)|^2 \delta[\hbar\omega - E_{\mathrm{L}}(r)]P(r)\mathrm{d}r \qquad (8)$$

where $g(r)$ is the carrier recombination probability, $P(r)$ is the distribution function for crystallite radius r, $f(r)$ is the oscillator strength and $E_{\mathrm{L}}(r)$ is the emission energy. Within the framework of the effective mass approximation, the parameter $|f(r)|^2$ is proportional to r^{-9} [25]. Following Kohno *et al.* [24], the explicit form of the

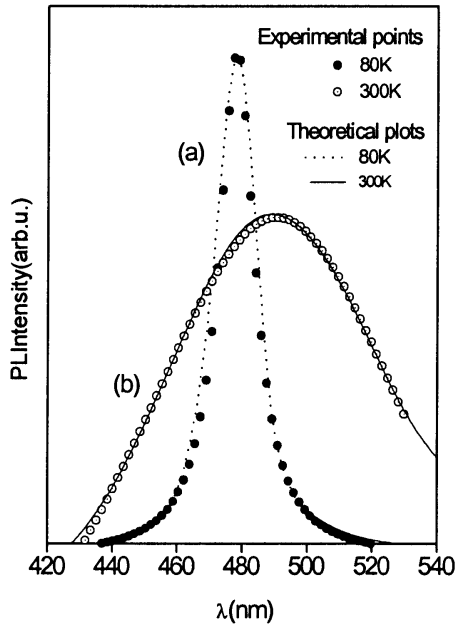

Fig. 8. Line shape analysis of the photoluminescence spectra recorded at (a) 80 K and (b) 300 K for a representative film with SiO_2:CdS=70:30 annealed at 373 K for 60 min. Theoretical best fits are shown for 80 K (- - -) and 300 K (——).

carrier recombination probability $g(r)$ is given by:

$$g(r) = 1 \qquad \text{for } r > \bar{r} \tag{9}$$

while for $r < \bar{r}$ we have

$$g(\bar{r}) = 2/\left[1 + (r/\bar{r})^2 \exp\left\{q\left(1/r^2 - 1/\bar{r}^2\right)\right\}\right] \tag{10}$$

where $q = E_d^2/3\hbar\rho V_S^3$, E_d is the deformation potential due to electron-phonon interaction, ρ is the mass density and V_S is the velocity of sound in the material and $P(r)$ is given by:

$$P(r) = (2\pi)^{-1/2} \Delta r^{-1} \exp\left[-(r - \bar{r})^2/2\Delta r^2\right] \tag{11}$$

where $\Delta r = (3KT/8\pi\sigma)^{1/2} = 0.3455(KT/\sigma)^{1/2}$, σ is the interface free energy per unit area, $\bar{r}$ is the average radii of particles and K is the Boltzmann constant.

Using equations [8–11], together with the parameters [21] $\rho = 5.28$ g/cm^3 $V_\mathrm{S} = 4.4$ km/sec (neglecting temperature variations of ρ and V_S), the theoretical fits of the line shape of the PL spectra recorded at 80 K and 300 K are shown in Figure 8 (curves a and b) respectively corresponding to the film (SiO_2:CdS=70:30) annealed at 373 K for 60 min. It may be observed that equation (8) describes the experimental observation quite faithfully. The estimated average crystallite size obtained from the above best fit to the PL line-shape, agreed well (Tab. 1) with those obtained from the blue shift and TEM studies. It may be observed that the Gaussian distribution of the particle size, as described in equation (11), culminates in better fit to the experimental PL spectrum than that is done with log-normal or Lifshitz-Slyozov distribution.

It is apparent that the PL line shapes become broad at higher temperature (curve b in Fig. 8) where phonon broadening would contribute significantly. As the distribution of the nanocrystallites would remain invariant for the film under study, the parameter that would control the line shape is the deformation potential (E_d). The best fit obtained for the PL peak recorded at 300 K indicated $E_\mathrm{d} \sim 3.0$ eV which is significantly lower than that obtained ($E_\mathrm{d} = 5.2$ eV) from the fit for PL spectrum recorded at 80 K. Thus, one may appreciate the strength of deformation potential in controlling the line shape of PL.

In reality, the exact nature of the emission mechanism in semiconductor nanocrystallites is very complex and a clear picture has not yet emerged. However, recent work [26,27] on this topic indicates that a significant role is played by the presence of complicated strain distribution in the vicinity of the nanocrystallites. Several fundamental mechanisms of carrier relaxation processes like multiphonon and Auger-like processes and their effects on the shape of the PL spectrum may be considered. In fact, the theoretical fit to the experimentally observed luminescence spectrum demands careful inclusion of all these effects which is under progress in our laboratory and will be reported in a future communication.

4 Conclusion

SiO_2/CdS films with different CdS contents (SiO_2:CdS=85:15, 80:20, 75:25 and 70:30) were deposited by the sol-gel technique onto soda-lime glass substrates. Variation of optical properties with crystallite size was studied with changes of annealing temperature (373–473 K). Variation of band gap for films with different CdS contents indicated that the signature of nanocrystallinity is retained throughout the range of our experimental conditions. With decreasing size of the nanocrystallites a blue shift of the band gap energy was observed. A thermal diffusion process controlled growth in the crystallite size with increasing annealing time and temperature. The average radii of the nanoparticles varied as the cube root of the annealing time but it showed exponential dependence on the inverse of annealing temperature.

Photoluminescence (PL) studies of the films indicated excitonic transitions. The line-shape of the PL peak could be explained by the combined effects of size distribution and phonon broadening. The peaks became broader at higher temperature where phonon broadening contributed significantly. The parameter which effectively controlled the line shape recorded at different temperatures was the deformation potential (E_d). The best theoretical fit for a representative film indicated $E_\mathrm{d} \sim 3.0$ eV and 5.2 eV for PL spectra recorded at 300 K and 80 K respectively. The present studies indicated that the emission mechanism in these composite films is very complex which demands careful inclusion of carrier relaxation processes.

References

1. L. Qi, H. Colfen, M. Antonietti, Nano Lett. **1**, 61 (2001)
2. S. Chaudhuri, A.K. Pal, *Proc. Indian National Science Academy, A* **67**, 131 (2001)
3. T. Tateno, *Proc. 6th International Symposium on Advanced Physical Fields, Growth of well defined nanostructures (March 6-9) (Tsukuba, Japan: National Research Inst. For Metals) p. 298 (2001)*
4. J.I. Lee, *Proc. 6th International Symposium on Advanced Physical Fields, Growth of well defined nanostructures (March 6-9) (Tsukuba, Japan: National Research Inst. For metals) p. 295 (2001)*
5. N. Tohge, M. Asuka, T. Minami, J. Non. Cryst. Solids **147&148**, 652 (1992)
6. H. Minti, M. Eyal, R. Reisfeld, Chem. Phys. Lett. **183**, 277 (1991)
7. S.K. Bera, S. Chaudhuri, R.P. Gupta, A.K. Pal, Thin Solid Films **382**, 86 (2001)
8. S.K. Bera, S. Chaudhuri, A.K. Pal, J. Phys. D Appl. Phys. **33**, 2320 (2000)
9. M. Guglielmi, A. Martucci, E. Menegazzo, J. Sol-Gel Technol. **8**, 1017 (1997)
10. A.K. Atta, P.K. Biswas, D. Ganguli, Mat. Lett. **15**, 99 (1992)
11. A.K. Atta, P.K. Biswas, D. Ganguli, *Polymers and Other Advanced Materials: Emerging Technologies and Business Oppertunities* (Plenum Press: New York, 1995) p. 645
12. R. Banerjee, R. Jayakrishnan, P. Ayyub, J. Phys. Cond. Matt. **12**, 10647 (2000)
13. M. Nogami, K. Nagasaka, M. Takata, J. Non-Cryst. Solids **122**, 101 (1990)
14. E. Cordoncillo, P. Escribano, G. Monros, M.A. Tena, V. Orera, J. Carda, J. Solid State Chem. **118**, 1 (1995)
15. R. Rossetti, J.L. Ellison, J.M. Gibson, L.E. Brus, J. Chem. Phys. **80**, 4464 (1984)
16. D. Bhattacharyya, S. Chaudhuri, A.K. Pal, Vacuum **43**, 309 (1992)
17. J.C. Manifacier, J. Gasiot, J.P. Fillard, J. Phys. E **9**, 1002 (1976)
18. L.E. Brus, J. Chem. Phys. **80**, 4403 (1994)
19. Y. Kayanuma, Phys. Rev. B **38**, 9797 (1988)
20. S.K. Mandal, S. Chaudhuri, A.K. Pal, Thin Solid Films **350**, 209 (1999)
21. *Landolt-Bornstein Numerical Data and Functional Relationships in Science and Technology* Vol. 22a (Berlin, Springer, 1987) 194 pp.
22. A.I. Ekimov, A.L. Efros, A.A. Onushchenko, Solid State Comm. **56**, 921 (1985)
23. T. Arai, H. Fujumura, J. Umezu, T. Ogawa, A. Fujii, Jpn J. Appl. Phys. **28**, 484 (1989)
24. K. Kohono, Y. Osaka, F. Toyomura, H. Katayama, Jpn J. Appl. Phys. **33**, 6616 (1994)
25. Y. Osaka, K. Tsunetems, F. Toyomura, H. Myorer, K. Kohno, Jpn J. Appl. Phys. **31**, L365 (1992)
26. S. Farad, R. Leon, D. Leonard, J.L. Merz, P.M. Petroff, Phys. Rev. B **52**, 5752 (1995)
27. A.L. Efros, V.A. Kherchenko, M. Rosen, Solid State Comm. **93**, 281 (1995)